JOURNAL OF
EMERGING INVESTIGATORS

Article

Optimizing airfoil shape for small, low speed, unmanned gliders: A homemade investigation

Teo Lara[1], Adriana Galvan[2]
[1] Decatur High School, Decatur, Georgia
[2] Emory University, Atlanta, Georgia

SUMMARY

Motivated by an interest to increase the efficiency of static airfoils, the objective of this study was to optimize airfoil lift generation based solely on airfoil shape. Enhancing the lift generated by airfoils without flaps can lead to longer flight times for unmanned gliders and possibly reduce fuel requirements for ground and air vehicles (1,2,3). We employed a Bernoullian model of airfoil lift generation to predict an optimized wing shape which was then constructed and compared with five others in a wind tunnel. We assembled airfoils from Styrofoam and conducted experiments in a small wind tunnel, measuring air speeds with a handheld anemometer. Our Bernoullian model related lift generation to the ratio of surface areas above and below an airfoil's chord, and because this ratio was maximized in our optimal airfoil, we predicted that this wing would generate more lift force than the other tested wings with lower ratios. However, we identified a variety of confounding variables including imperfections in wing constructions, turbulent airflow and air resistance within the wind tunnel, and low resolution of the anemometer, all of which contributed to unpredicted and unreliable results. Moreover, we concluded that our mathematical model was not rigorous enough to be generalized to a wider set of experimental conditions. Despite these shortcomings, our results did point to a correlation between airfoil shape and lift generation, and will allow for more informed, less-error prone future studies.

INTRODUCTION

This investigation aimed to build on the existing knowledge base regarding the relationship of airfoil shape and lift generation (1). It is well known that airfoil shape can drastically impact lift generation, and most manned aircraft alter their wings midflight using flaps to this end (1,2). Our study is constrained to the static, unmoving airfoil case, aiming to identify the airfoil shape that generated the most lift for small, unnamed vehicles flying at low speeds and altitudes. While not widely applicable to larger aircraft, our results aimed to improve flight times for uncrewed gliders, and perhaps lay the groundwork for more general static airfoil shape optimizations that could be used in more complex systems (2). Outside of flying vehicles and devices, optimizing lift generation for static airfoils could also have applications in heavy ground vehicles, serving to generate lift force and reduce weight, increasing fuel efficiency (3).

Our study consisted of two portions, mathematically optimizing airfoil shapes based on the relationship of lift force and airfoil surface area derived from Bernoulli's Principle and comparing this optimized airfoil to other wing designs in a small wind tunnel. The results, discussion, and materials and methods sections of this paper are all divided into both mathematical and experimental sections.

RESULTS

Mathematical Modeling

Generally, the lift force of an airfoil (F_L) is governed by the lift equation (eq. 1), depending on the lift coefficient (C_L), fluid density (ρ), true air speed (v), and projected wing area (s).

$$F_L = C_L \cdot \frac{1}{2}\rho \cdot v^2 \cdot s \quad (eq.1)$$

Of these factors, the lift coefficient is the only one that cannot be directly measured and is instead experimentally determined with respect to the angle of attack and airfoil shape (4). The angle of attack describes the airfoil angle with respect to incoming fluid and, by adjusting this angle using flaps, the lift coefficient can be significantly altered (5,6). But for the static airfoil case, the lift coefficient is constant, and because this value must be experimentally determined, an alternative equation stemming from Bernoulli's Principle was used to optimize lift generation.

Bernoulli's Principle describes the relationship between fluid velocity and pressure. In Bernoulli's equation (eq. 2), the first term variables (v_1) represent values below the wing, while second term variables, (v_2) represent values above the wing. P represents pressure (N/m^2), ρ measures fluid density (kg/m^3), v represents the velocity of the flowing fluid (m/s), g is the acceleration due to gravity (m/s^2), h measures the height of the fluid flow from sea level (m).

$$P = \frac{\rho}{2}(v_2^2 - v_1^2 + 2gh_2 - 2gh_1) \quad (eq.2)$$

Change in pressure is equivalent to the net force over the area, and therefore the lift force, F_L (N), was found by rewriting equation 2, where A is the total surface area of the airfoil (m^2) (eq. 3). Bernoulli's principle relates force generation to a pressure differential to a velocity differential, but does not explain why this velocity differential occurs, and is thus an incomplete model of airfoil lift. However, for the purposes of this experiment, we measured velocities above and below the wings to calculate lift, hence the model was sufficiently applicable, and no explanation was required. Note that the equation based on Bernoulli's principle (eq. 2) and the more general lift formula (eq. 1) both calculate lift force and are interchangeable as long as wind speed and air pressure are low, flow is non-turbulent, and the angle of attack is zero.

Flow was assumed to be non-turbulent in this experiment. The surface must also be a simple, bounded surface that does not pass over itself for equations to be applicable (4,7).

$$F_L = \frac{A\rho}{2}(v_2^2 - v_1^2 + 2gh_2 - 2gh_1) \quad (eq.3)$$

Using this lift function, relating lift generation to airfoil surface area, the optimally lift generating air foil was found **(Table 1)**, and its lift creation was described as a function of the incoming true airspeed (eq. 4).

$$F_L(v) = 0.00250v^2 + 0.01941 \quad (eq.4)$$

This and all tested airfoils have several defining characteristics: chord length, *L* (m), maximum length from the chord to the bottom of the airfoil, T_1 (m), and maximum length from the chord to the top, T_2 (m) (Figure 1) (8). Airfoils also have points along the chord with maximal thickness, these being *EL* above the chord and *GL* below the chord, *E* and *G* are unitless multipliers of the chord length. By varying these parameters, the five other comparison airfoils were created **(Table 2)**.

Airfoil Shape Assessment

To assess lift generation, six experimental airfoils were tested in a small wind tunnel. Airfoils, constructed out of Styrofoam were suspended in the middle of the wind tunnel with thin rods. A handheld anemometer was inserted into the wind tunnel and was used to measure airspeeds above and below airfoils (**Figure 2** and **Table 3**). The constants of fluid density, fan wind speed, and gravitational acceleration were controlled using identical experimental procedures for all trials (for each wing, n = 300 measurements conducted, both above and below the wing). The six tested airfoils had distinct characteristics and lift forces were calculated for each of them using the Bernoullian model (**Figure 1** and **Table 4**). Wing 1 was the optimized design, wings 2 through 5 changed the airfoils *E* and *G* values to serve as comparisons to the optimized wing and wing 6 acted as a control, a symmetric wing that should have generated much less lift than any of the other airfoils. *v* was treated as 5.66 m/s, the air speed of the empty wind tunnel when the fan was turned on.

All wind speed data sets were found to be normally distributed under a Shapiro-Wilk expanded test at the 99% confidence level (p-values ~ 0.01, all cases), allowing comparisons of wind speed for each airfoil utilizing a standard two-tailed two *t*-test.

Maximum Thickness of airfoil below chord, T_1 (m)	Maximum Thickness of airfoil above chord, T_2 (m)	*G*	*E*
0.00500	0.03204	1	0.07629

Table 2: Calculated values for maximal lift generation. Table showing T_1, maximum upper thickness, T_2, maximum lower thickness, *G*, and *E* values for airfoil results in maximal lift according to the mathematical model.

The means for the wind speeds of the upper and lower sections of the wind tunnel were not found to be significantly different at the 95% confidence level (p-values ~ 0.02, two-tailed t-test). The above and below measurements of the symmetric control wing (Wing 6), were not significantly different from each other at the same level (p-values ~ 0.02, two-tailed t-test). Therefore, inconsistent wind speeds in different sections of the tunnel were eliminated as an error source for the other data points. Air speed measurements taken above and below wings 1 through 5, were found to be significantly different at the 99.9% confidence level, indicating that the experimental airfoils did affect wind speeds (p-values ~ 0.001, two-tailed t-tests, for all cases) **(Figure 2)**.

The anemometer resolution of 0.1 m/s created an absolute error margin in the wind speed values and calculated lift generation, meaning that any measured wind speed could be inaccurate by up to 0.05 m/s, an error that only augmented as lift forces were calculated. This error margin ranged from 40% to 780% proportional to the lift force test statistic (**Figure 3** and **Table 3**), and, momentarily ignoring these margins, all experimentally obtained lift forces were at least 10% off from the predicted values, and at most, over 100% off in the case of wings 1 and 2 **(Figure 3)**. In some cases, a higher wind speed was observed under the wing than over, resulting in a negative calculated lift force for Wings 1 and 2. These unexpected results and limitations in measurement equipment did not allow us to reliably determine the optimal airfoil shape from the collected data.

DISCUSSION

The aim of this study was to model an optimized airfoil shape to maximize lift generation in an unmanned glider and experimentally compare the optimized airfoil with others in a

ρ, Fluid Density, under normal conditions at experiment location (10)	1.22404 kg/m^3
g, Acceleration Due to Gravity, under normal conditions at experiment location	9.80567 m/s^2
L, Chord Length	0.42 m
V, Angle of Separation	6°
2*t*, Minimum Total Airfoil Thickness	0.01 m
Airfoil Width	0.0508 m

Table 1: Values of constants used in experiment. Table depicting values of constants used in all formulas and calculations throughout experiment.

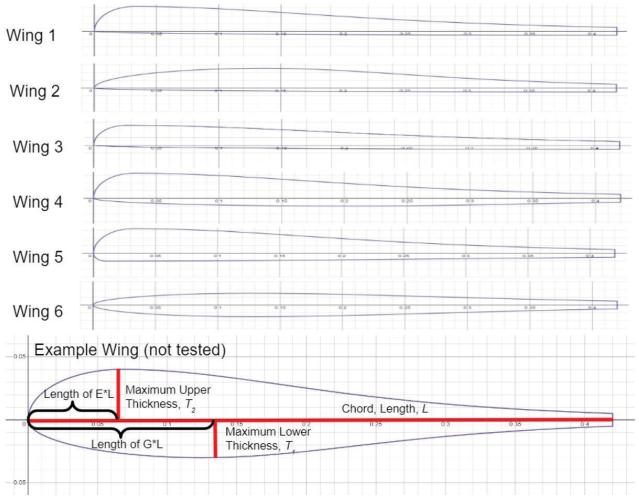

Figure 1: Airfoil cross-section diagram. Cross sections of all tested airfoils as well as an example airfoil in which the following parameters are indicated: maximum upper thickness (T_1), maximum lower thickness (T_2), length of *GL*, length of *EL*, and chord length (*L*). Horizontal and vertical axis measured in meters. Wing 1: optimized wing shape, wing 2: longer *EL* section over wing top, wing 3: longer *EL* section over wing bottom, wing 4: shorter *GL* section over wing bottom, wing 5: drastically shorter *GL* section over wing bottom, wing 6: symmetric control wing.

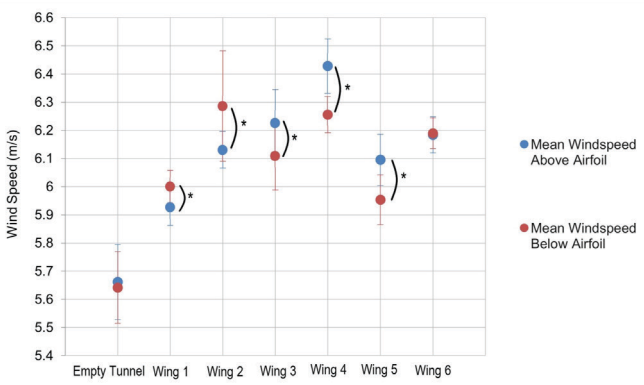

Figure 2: Wind speeds measured for all airfoils. The average wind speed measured above (blue) and below (red) for the six experimental wings. Error bars represent the standard deviation. * $p < 0.001$, two tailed standard *t*-test.

wind tunnel. We first discuss the mathematical model used, followed by a discussion of the experimental results obtained when assessing airfoil shapes.

Mathematical Modeling

Assuming a Bernoullian model is maintained, models for airfoil shape could be improved through more general equations. The tested models were only a single subset of wing shapes, and without an equation set that allows for all shapes, complete optimization cannot be assumed. A more robust equation set, with more piecewise sections or differential curves, could represent a broader array of airfoil shapes could more effectively determine the optimal wing shape. Alternatively, airfoils could be assembled without the restrains of equations, having functions modeled after their likeness and then optimized.

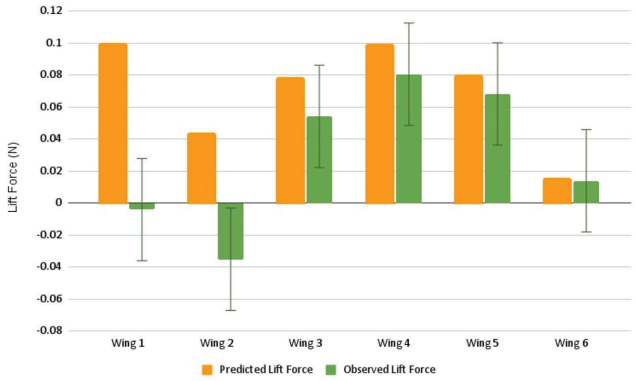

Figure 3: Comparison of predicted and observed mean lift force. The graph compares the predicted lift force generation (orange bars) with the observed mean lift force generation (green bars). Error bars indicate error in lift force calculations due to anemometer inaccuracies. Values are in newtons.

Even if wing equations were expanded, the Bernoullian model of lift generation is incomplete and provides only a partial description of air flow. This model ignored variations of wind speeds approaching the airfoil, contraflow, vacuums from areas of different pressure regions, and non-direct winds that impacted airfoils at angles. This model also assumed that air in the wind tunnel and over foils was non-turbulent. At such low wind speeds turbulence is likely, and thus, this model is inaccurate for this application.

In addition, calculations for the angle of separation were omitted for simplicity, and wings were assumed to have an axis with unchanging cross sections. It is possible that air separated from the back half of airfoils, impacting the results measured. Without definitively knowing airflow patterns around foils, calculated lift values were most likely inaccurate. Mathematically expressing a more inclusive Newtonian approach may be possible, but computer simulations could be more accurate (13,14). Simulated air molecules would allow for greater control of variables such as pressure, temperature, wind speed, and other factors. These more comprehensive models would allow for a greater number of experimental airfoils, as well as increased confidence in complete airfoil optimization.

Experimental Discussion

Our experimental results showed that the optimized airfoil (Wing 1) did not generate the highest lift force. We believe that this is due to the importance of several confounding variables and uncontrolled factors inherent to our experiment, including the wind tunnel design, airfoil construction methods, airfoil materials, and uncontrolled turbulent flow present during experimentation. Despite the bottom sections of airfoils one, two and three having identical shapes, the wind speeds below these airfoils were found to be significantly different when compared to each other (p-values ~ 0.001, two-tailed *t*-tests, for all cases). Similarly, statistically different wind speeds were measured over the tops of foils four and five, despite these wings having identical top sections (p-values ~ 0.001, two-tailed *t*-tests, for all cases). Theoretically, wind speed values over identical wing shapes should not have resulted in statistically different values, and because this is not the case, we assume that a confounding factor impacted the data. This

factor could be due to turbulent flow, inaccuracies in airfoil constructions, uneven wing placements with the wind tunnel, or a combination of all these.

A focusing cone that was too narrow resulted in air flow outside the wind tunnel that may have disrupted the entrance flow. A larger focusing cone to capture all incoming air or a fan placed inside the tube would allow for all incoming air to enter the tube and a wind tunnel with perfect seals to attach the measuring anemometer could also reduce turbulence. The efficacy of the focusing tubes in creating laminar flow was also questionable. These tubes were too short with too many gaps between them to create a fully smooth flow. Without further tests into laminar flow, it cannot be determined that they did not influence the results, and, as aforementioned, a Bernoullian model at these wind speeds is inapplicable without non-turbulent flow (11). To improve laminar flow, longer tubes, with less spacing between them, could aid in focusing the air, but before experimentation, smoke tests should be performed to analyze wind direction and reduce turbulence (12).

The airfoil construction also likely impacted results. Given the nature of Styrofoam, the fabrication of calculated wing shapes was inaccurate, creating differences between estimated and observed lift values. Airfoil support holes were not symmetric on either side of the wind tunnel, forcing wings into positions that were not parallel to oncoming air. Because lift calculations assumed an attack angle of zero, these equations did not serve as accurate predictors. More rigid materials cut with more precise methods would help reduce these inaccuracies. For future experiments we recommend machine cut wooden or aluminum airfoils, or 3D printed wings made from non-porous plastics.

Furthermore, the anemometer's low resolution, propagating to proportionally large margins of error in lift forces **(Table 3)** made conclusions difficult to draw. With such error, the accuracies of lift force predictions are unclear, and even if no other confounding variables were present, the optimal airfoil would still be undeterminable for this reason. More accurate anemometers, with much higher resolutions are critical for similar experiments, or by increasing airfoil sizes and differences in wind speeds, the proportional error of an anemometer's resolution can also be reduced.

Although the prescribed objective of determining the airfoil shape that generated the most lift was not achieved due to the experimental limitations, some significant takeaways can be gathered. Because air speeds over and under all wings were significantly different, while the wind speeds for both the top and bottom of the wind tunnel were not, it can be concluded that airfoil shape does affect wind speed, and different shapes result in different speeds. Even if the changes in lift between experimental foils were not drastic in this experiment, on larger wings, differences in lift generation could be more relevant, and further exploration into airfoil optimization could result in more efficient planes, gliders, and even heavy ground vehicles, reduced fuel usage and increasing efficiency (3).

METHODS

Mathematical Modeling

From Bernoulli's principle, a relation of airfoil surface area, windspeed above, windspeed below, and lift force was derived (eq. 3). Since v_1 and v_2 represent velocities over and under the wing, they can be rewritten in terms of v, L, A_1, and A_2, where A_1 and A_2 represent the length of the lower and upper wing surfaces, respectively (eqs. 5, 6).

$$v_1{}^2 = \left(\frac{vA_1}{L}\right)^2 \quad (eq.5) \qquad v_2{}^2 = \left(\frac{vA_2}{L}\right)^2 \quad (eq.6)$$

Airfoil	Mean wind speed, over airfoil, ± 0.05 m/s error margin (m/s)	Standard deviation of wind speed, over airfoil (m/s)	Mean wind speed, under airfoil, ± 0.5 (m/s)	Standard deviation of wind speed, under airfoil (m/s)	Calculated mean lift generation, ± 0.3 (N)	Percent error margin in lift generation
Wind Speed of Empty Tunnel	5.66	0.13	5.64	0.13	N/A	N/A
1- Hypothetically Optimized	5.93	0.06	6.00	0.06	0.00	± 783%
2- Longer Streamline Over Top	6.13	0.06	6.29	0.20	-0.04	± 93.1%
3- Shorter Streamline Over Top	6.23	0.12	6.11	0.12	0.05	± 60.6%
4- Slightly Shorter Streamline Over Bottom	6.43	0.10	6.26	0.06	0.08	± 42.1%
5- Drastically Shorter Streamline Over Bottom	6.10	0.09	5.96	0.09	0.07	± 47.5%
6- Symmetric	6.18	0.06	6.19	0.05	0.01	± 239%

Table 3: Parameters of wind speed and lift generation measured for various airfoil shapes. Table containing mean and standard deviation statistics for data collected on all airfoils, with absolute error for each data value. The mean lift force calculated using the mean value of wind speeds above and below airfoils is also represented, with both absolute and percent error margins. All values are rounded to two decimal places.

For mathematical simplicity, airfoils are assumed to have a constant cross section in the axis perpendicular to the cross section **(Figure 1)**. This assumption allows for a constant width through airfoils, and instead of adjusting surface area, A, lengths A_1 and A_2 are modified to maximize lift, and A can be found by multiplying the sum of A_1 and A_2 by airfoil width, w (m). The thickness of the wing can therefore be rewritten as the sum of T_1 and T_2 (eq. 7).

$$F_L = w\frac{(A_2 + A_1)\rho}{2}\left(\left(\frac{vA_2}{L}\right)^2 - \left(\frac{vA_1}{L}\right)^2 + 2g(T_2 + T_1)\right) \quad (eq.7)$$

Airfoils could have many shapes and were designed using two functions of l, $f_1(l)$ and $f_2(l)$ which return values for the thickness of the bottom and top part of the airfoil, respectively, based upon a position l along the chord, L. These are defined piecewise (eqs. 8, 9).

$$f_1(l) = \begin{cases} -\sqrt{-\frac{T_1^2}{GL}\left(\frac{(l-GL)^2}{GL} - GL\right)}, & 0 < l \le GL \\ -T_1\,\mathrm{sech}\left(\frac{\cosh^{-1}\left(\frac{T_1}{t}\right)}{(L-GL)}(l-GL)\right), & GL < l < L \end{cases} \quad f_2(l) = \begin{cases} \sqrt{-\frac{T_2^2}{EL}\left(\frac{(l-EL)^2}{EL} - EL\right)}, & 0 < l \le EL \quad (eq.8) \\ T_2\,\mathrm{sech}\left(\frac{\cosh^{-1}\left(\frac{T_2}{t}\right)}{(L-EL)}(l-EL)\right), & EL < l < L \quad (eq.9) \end{cases}$$

G and E are unitless values, measuring the ratio of $f_1^{-1}(T_1)$ and $f_2^{-1}(T_2)$ about L, respectively. Since the limit of these equations as l approaches infinity is zero, t is a value representing the minimum amount of distance between the chord and end of airfoil curves.

Using length integrals, A_1 and A_2 were rewritten as functions of G and E (eqs. 10, 11). Although total airfoil lengths include t sections, it was not added into the length formula because fluid does not flow over this portion of the wing. With these equations, F was rewritten as a function of E and G (eq. 12).

$$A_1(G) = \int_0^L \sqrt{1 + \left(\frac{d}{dl}f_1(l)\right)^2}\,dl \quad (eq.10) \qquad A_2(E) = \int_0^L \sqrt{1 + \left(\frac{d}{dl}f_2(l)\right)^2}\,dl \quad (eq.11)$$

$$F(E,G) = w\frac{\rho}{2}\left(A_2(E) + A_1(G)\right)\left(\left(\frac{vA_2(E)}{L}\right)^2 - \left(\frac{vA_1(G)}{L}\right)^2 + 2g(T_2 + T_1)\right) \quad (eq.12)$$

Parameters were then allocated to create a more realistic model. The wing front must be formed from two ellipses with horizontal radii greater than or equal to their vertical radii. The drag coefficient of a semi-circular prism is around 1.15 and increases drastically if the shape becomes steeper and less circular (9). To reduce drag, and thus increase net lift, the front of the wing must be horizontally longer than a half-circle (eqs. 13,14).

$$GL \ge f_1(GL) \Rightarrow GL \ge T_1 \quad (eq.13) \qquad EL \ge f_1(EL) \Rightarrow EL \ge T_2 \quad (eq.14)$$

For the back of the wing, fluid must continue to flow over the surface. If there is an angle that is too steep, greater than V degrees, then pressure acting on air particles will be insufficient to keep them attached to the wing, resulting in fluid separation. Fluid separation causes turbulent flow, meaning less lift. The angle of separation V is determined experimentally through computer simulations for most airfoil designs and depends on many factors, the most important being air pressure P and air speed v, as P and v increase, so does V (7,9). In this model, with low wind speeds and pressures, V is set to a low value, 6° (eqs. 15,16).

$$\frac{d}{dl}f_1\left(\left(\frac{d^2}{dl^2}f_1\right)^{-1}(0)\right) \le \tan\left(\frac{\pi V}{180}\right)\{0 < G < 1\} \Rightarrow G \le 1 - \frac{T_1\cosh^{-1}\left(\frac{T_1}{t}\right)}{2L\tan\left(\frac{\pi V}{180}\right)}\{0 < G < 1\} \quad (eq.15)$$

$$\frac{d}{dl}f_2\left(\left(\frac{d^2}{dl^2}f_2\right)^{-1}(0)\right) \le -\tan\left(\frac{\pi V}{180}\right)\{0 < E < 1\} \Rightarrow E \le 1 - \frac{T_2\cosh^{-1}\left(\frac{T_2}{t}\right)}{2L\tan\left(\frac{\pi V}{180}\right)}\{0 < E < 1\} \quad (eq.16)$$

Using these parameters, the values of E, G, T_1, and T_2 that will maximize lift force were found (eqs 17, 18).

$$c(T_1) = \frac{d}{dT_1}F(E,G),\ T_1 = c^{-1}(0),\ G = 1 - \frac{T_1\cosh^{-1}\left(\frac{T_1}{t}\right)}{2L\tan\left(\frac{\pi V}{180}\right)},\ E = \frac{T_2}{L} \quad (eq.17)$$

$$b(T_2) = \frac{L}{T_2} - \frac{\cosh^{-1}\left(\frac{T_2}{t}\right)}{2\tan\left(\frac{\pi V}{180}\right)} - 1,\ T_2 = b^{-1}(0) \quad (eq.18)$$

Based on the available materials for this study, a chord of length 42 cm was used, and a minimum amount of distance between the chord and the end of the airfoil curve, t, was set to 0.5 cm. t was minimized to allow for the longest possible airfoil surfaces, but due to material constraints, a smaller t could not be achieved without making airfoils too fragile for wind tunnel testing. Constants, including fluid density and gravitational acceleration, were found and with these values, and V remaining at 6°, the dimensions of the hypothetically optimal airfoil shape was determined (**Table 1** and **Table 2**). While fluid density and gravitational acceleration may not be constant over all wing portions, changes in these values are negligible for these calculations (10). Calculations were done using Desmos Graphing Calculator (desmos.com/calculator). Statistics were calculated in Microsoft Excel 2019.

Construction of Wind Tunnel and Airfoil Shape Assessment

All airfoils were made from Styrofoam wrapped in duct tape to cover any holes. The tape was wrapped across the airfoils' chords, perpendicular to incoming air flow and ensuring a smooth air flow around wings. Due to the nature of curves, the airfoil shapes were not exactly replicated when being hand cut, but a printed cross-section of the airfoil shape was used as a template, maximizing accuracy. Airfoils were 5.08 cm wide and were assembled in two identical 2.54 cm wide sections.

The airfoils were assessed in a wind tunnel, powered by a 0.91 m diameter industrial fan (Honeywell Commercial Grade HV-180 Floor Fan). The tunnel was constructed out of a steel duct pipe with a 30.48 cm diameter. A focusing cone made from card stock, with the same maximum diameter as the fan (0.91 m), and the same minimum diameter as the tunnel (30.48 cm), with a length of 25 cm, brought air into the tunnel from the fan. An array of cardboard tubes inside the tunnel, each with a radius of 3.8 cm, focused the air into a laminar flow (12). The airfoil was placed 30.48 cm after this section, and rectangular cuts in the duct tube (20 cm by 9 cm) above and below the airfoil allowed for the insertion of an anemometer (Holdpeak HP-866B-APP anemometer, resolution = 0.1 m/s) to measure the wind speed **(Figure 4)**.

The fan was then turned on and measurements of true air speed were made without an airfoil in the chamber. Five measurements (30 seconds long each, with 60 measurements made in this period) were taken, both at the upper and lower tube portions. This resulted in 300 data points for each portion of the tube. Five trials of 60 measurements combined into 300 measurements accounting for both wind speed and fan variability during and between trials.

The wind tunnel had two holes from which measurements were taken; while measurements were taken in the upper portion of the tunnel, the lower hole was firmly sealed from inside and outside with duct tape. Likewise for the upper hole when measurements were done from the bottom.

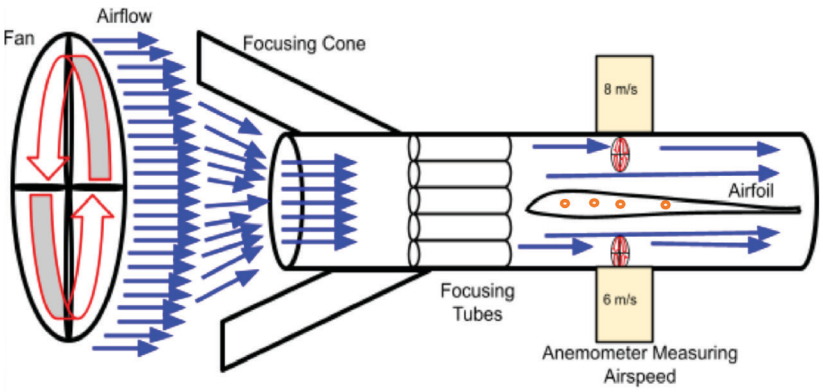

Figure 4: Diagram of experimental setup. The diagram features the wind tunnel, focusing cone, fan, focusing tubes, sticks holding airfoil (orange circles), air foil, and anemometer locations (red circles). The airflow is represented by blue arrows passing through wind tunnel.

Measurements were taken with a handheld anemometer, inserted into the hole. If measurements taken at the top and bottom of tunnel were discrepant, the wind tunnel was modified until a constant air speed was achieved in all portions of the tunnel. A constant air speed throughout ensured accuracy for measurements involving airfoils.

After the control trials with an empty wind tunnel were conducted and the tunnel was properly calibrated, experimental trials for the six airfoils took place. The airfoils were placed in the center of the tunnel, suspended by four thin wooden sticks passing through the airfoils (orange circles, **Figure 4**). These sticks were placed parallel to the bottom edge of the wind tunnel and were vertically bisecting the diameter of the tube to create an angle of attack of zero for the airfoil. The airfoil's chord was parallel to the tunnel's walls and was in the center of the tunnel. After the airfoil was situated, the fan was once again turned on and measurements of air speed above and below the wing were recorded, with five trials for each measurement, with identical time frames as described previously, yielding 300 points over five total minutes. This process was repeated for all experimental airfoil shapes. All experiments were done on the same day at the same location, to minimize variability of conditions.

ACKNOWLEDGMENTS

We thank John Chesnut (Decatur High School, Decatur, GA) and Dr. Cassy Smith (Decatur High School, Decatur, GA) for providing research and formatting guidance.

Received: June 18, 2022
Accepted: October 20, 2022
Published: March 30, 2023

REFERENCES

1. Abbott, Ira H., and Von Doenhoff A. E. *Theory of Wing Sections.* Dover Publications., 1959.
2. Muller, J. "Reducing Fuel Consumption by Aerofoil Optimization." *Juniper Online Journal of Material Science,* vol. 6, Jul 2021, doi: 10.19080/JOJMS.2021.06.555692.
3. Priyadarshini, S, *et al.* "Use of Aerodynamic Lift in Increasing the Fuel Efficiency of Heavy Vehicles." *Journal of Mechanical and Civil Engineering,* vol. 12, Aug, 2015, pp 39-42
4. Houghton, E. L., *et al. Aerodynamics for Engineering Students.* 7th ed. Butterworth-Heinemann, 2017.
5. Hall, N. "Lift Equation." *Glenn Research Center,* National Aeronautics and Space Administration, 13 May 2021, www.grc.nasa.gov/www/k-12/airplane/lifteq.html. Accessed 13 Oct. 2021.
6. Lopez, D. R. "Student Airfoil Interactive." *Glenn Research Center,* National Aeronautics and Space Administration, 13 May 2021, www1.grc.nasa.gov/beginners-guide-to-aeronautics/foilsimstudent/. Accessed 13 Oct 2021.
7. Nakamura, M. "Airfoil." *Reports on How Things Work,* Massachusetts Institute of Technology, web.mit.edu/2.972/www/reports/airfoil/airfoil.html. Accessed 13 Oct 2021.
8. "NACA 5 digit airfoil generator." *Airfoil Tools,* airfoiltools.com/airfoil/naca5digit. Accessed 13 Oct 2021.
9. Hall, N. "What is Drag?" *Glenn Research Center,* National Aeronautics and Space Administration, 13 May 2021, www.grc.nasa.gov/www/k-12/airplane/drag1.html. Accessed 13 Oct 2021.
10. "Density of Air." Chemeurope, www.chemeurope.com/en/encyclopedia/Density_of_air.html. Accessed 27 Nov 2021.
11. "Reynolds Number." Encyclopedia Britannica, 18 Oct 2019, www.britannica.com/science/Reynolds-number. Accessed 6 Oct 2022.
12. "What is Laminar Flow?" Simscale, 2 Sep 2021, www.simscale.com/docs/simwiki/cfd-computational-fluid-dynamics/what-is-laminar-flow/. Accessed 15 Oct 2021.
13. Hall, N. "Bernoulli and Newton." *Glenn Research Center,* National Aeronautics and Space Administration, 13 May 2021, www.grc.nasa.gov/www/k-12/airplane/bernnew.html. Accessed 14 Oct 2021.
14. Liu, T. "Evolutionary Understanding of Airfoil Lift." *Advances in Aerodynamics,* vol. 3, no. 37, Dec. 2021, doi:10.1186/s42774-021-00089-4.

Copyright: © 2023 Lara and Galvan. All JEI articles are distributed under the attribution non-commercial, no derivative license (http://creativecommons.org/licenses/by-nc-nd/3.0/). This means that anyone is free to share, copy and distribute an unaltered article for non-commercial purposes provided the original author and source is credited.